Development of Bifacial p-Type and n-Type Solar Cells with Reduced Thermal Processing and Comparison of Bifaciality Coefficients

Izete Zanesco, Adriano Moehlecke, Fábio André Biazetto, Augusto dos Santos Kochenborger, Lucas Teixeira Caçapietra Pires da Silva, João Victor Zanatta Britto, Thais Crestani, Daniel Augusto Krieger Coutinho and Vítor Gomes de Venuto

Solar Energy Technology Nucleus, School of Technology, Pontifical Catholic University of Rio Grande do Sul – PUCRS, Porto Alegre (Brazil)

Abstract

Bifacial n-type TOPCon and p-type PERC solar cells represent a market share of 90%. The reduction of production costs is a goal of the industry, and a way to address this challenge is to develop a manufacturing process with a reduced number of steps. Considering these facts, the aim of this study is to compare and analyse the bifaciality coefficients of p-type and n-type bifacial solar cells developed with the diffusion of boron and phosphorus in a single thermal step. The co-diffusion of dopants was performed according to the patent application BR1020180085760. The sheet resistance (R_{sh}) and I-V characteristics of p-type and n-type bifacial solar cells produced with boron diffusion temperatures ranging from 940 - 970 °C were measured to determine the bifaciality coefficients. For both types of substrates, the R_{sh} of the emitters was higher than the R_{sh} of the back surface field, and the phosphorus-doped layer was affected by the boron diffusion temperature. The short-circuit current density (J_{sc}) of p-type bifacial solar cells with incident irradiance on the boron-BSF was low. Consequently, the J_{sc} and the maximum power output bifaciality coefficients of the p-type devices were approximately 0.6, lower than those of the n-type solar cells, which were close to 1.0. The results demonstrated that the bifaciality coefficients of commercial n-type TOPCon solar cells have the potential to be improved from 0.8 to approximately 1.0.

Keywords: Bifacial solar cells, p-type and n-type solar cells, reduced thermal steps, bifaciality coefficients

1. Introduction

The first bifacial solar cell with a p^+np^+ structure was reported in the 1960s (Cuevas, 2005). In the 1970s, bifacial solar cells with a conversion efficiency of 17.2% were reported (Arndt et al., 1975). Two decades passed to achieve efficiencies of 18.1% and 19.1% (Moehlecke et al., 1994) in the p^+nn^+ configuration and incident irradiance on the boron-doped emitter and phosphorus-doped back surface field (BSF), respectively. This solar cell was passivated with a silicon oxide layer thermally grown on both faces. Three years later, in 1997, with this configuration and floating junction concept to reduce recombination, Glunz et al. (1997) reported efficiencies of 20.6% and 20.2% under emitter and BSF illumination, respectively.

The passivated emitter and rear solar cell (PERC) was reported in 1989, with an efficiency of 21.8%, and was the dominant commercial technology in the last decade (Green, 2015). This solar cell technology represented 35% of the market share in 2024 (VDMA, 2025). The main features of the PERC configuration are the reduction of minority charge carrier recombination and the increase of internal reflectance at the rear side. PERC solar cells are manufactured in p-type monocrystalline silicon wafers with passivation layers of AlO_x and SiN_x (Wei et al., 2024). Currently, tunnel oxide passivated contact solar cells (TOPCon) are the dominant technology, accounting for 55% of the market share (VDMA, 2025). TOPCon solar cells manufactured in n-type monocrystalline silicon wafers have high-quality passivation on the rear side, which includes ultrathin tunnel silicon oxide and phosphorous-doped polycrystalline silicon layers (Kafle et al., 2021; Ullah et al., 2023). The efficiency of mass production PERC solar cells is approximately 23–24% (VDMA, 2025; Wang et

© 2026. The Authors. Published by International Solar Energy Society
Selection and/or peer review under responsibility of Scientific Committee
10.18086/swc.2025.03.20 Available at http://proceedings.ises.org

al., 2024; Huang et al., 2024; Yuan et al., 2025). This efficiency is lower than that of TOPCon devices, which is 25–26% (VDMA, 2025; Wang et al., 2024; Linke et al., 2025; Wang et al., 2025). Both solar cell structures enable the manufacturing of bifacial devices. Currently, bifacial solar cells are the standard technology, with a market share of approximately 90% (VDMA, 2025).

The passivated emitter and rear totally diffused (PERT) solar cell is one of the configurations of the PERC family. Bifacial PERT solar cells can be developed in p-type or n-type crystalline silicon wafers with n^+pp^+ or p^+nn^+ structures. As in TOPCon devices, phosphorus diffusion into one side of a silicon wafer and boron diffusion into the other side are required to form the emitter and the back surface field.

The n-type substrate presents several advantages. The minority carrier lifetime in n-type silicon wafers is higher than in p-type substrates (Sugiura et al., 2021). Metallic impurities are more effective in capturing electrons than holes because of their positive charge, leading to a lower minority carrier lifetime in p-type silicon than in n-type silicon (Macdonald et al., 2012). Therefore, n-type solar cells are less affected by metallic contaminants present in silicon substrate or introduced during processing. Additionally, the mobility of holes, which are minority carriers in n-type substrates, is lower than that of electrons, which are minority carriers in p-type silicon. In bifacial solar cells, the minority carrier diffusion length should be 2-3 times the thickness of the solar cell (Moehlecke et al., 1995; Jimeno et al., 2007) and should be higher in p-type solar cells than in n-type devices (Moehlecke et al., 1995).

Zhang et al. (2020) developed bifacial p-type PERC solar cells with efficiencies of 22% and 15% measured under incident irradiance on the emitter and rear sides, respectively. The selective emitter was laser doped, and an optimized silicon nitride layer was deposited on the rear side. Using a method based on the simultaneous formation of a phosphorus-doped emitter and a boron-doped BSF, Khelifati et al. (2020) obtained an efficiency of 12.8%, under incident irradiance on the emitter side and a bifaciality coefficient of 52.5%. In n-type substrates, Ingenito et al. (2023) reported an efficiency of 22.8% under incident irradiance on the emitter. The bifacial n-type solar cells were produced with a homogeneous boron emitter and phosphorus-doped polysilicon deposited by DC sputtering on thin silicon oxide. A high bifaciality coefficient of 94.3% was achieved in TOPCon solar cells, incorporating new concepts of processing and passivation layers of SiO_2/poly-Si/Al_2O_3/SiN_x under silver electrodes and Al_2O_3/SiN_x on the rear side (Feng et al., 2025). The simulation of rear emitter TOPCon solar cells revealed that the strategy to improve device performance is to reduce carrier recombination in the front surface field (FSF) and in the contact area. The optimized device by simulation demonstrated the potential of achieving a 26.62% efficiency under incident irradiance on the FSF (Zhou et al., 2024).

In the manufacturing process of solar cells, reducing the number of thermal steps to implement phosphorus diffusion into one side of the silicon wafer and boron diffusion into the other face is a way to decrease the production cost. Wei et al. (2017) developed bifacial n-type solar cells with boron and phosphorus co-diffusion. Boron paste was deposited via the spin-coating method, and the emitter and BSF were produced in one co-diffusion process. The boron paste acted as a barrier to phosphorus diffusion. The efficiencies achieved under front and rear side illumination were 20.4% and 18.3%, respectively. Yin et al. (2020) developed n-type bifacial solar cells with the diffusion of boron and phosphorus in the same thermal step and with a laser-doped selective BSF. The emitter was formed by depositing a boron silicate glass layer using the atmospheric pressure chemical vapour deposition (APCVD) method. The efficiency achieved under incident irradiance on the selective phosphorus-doped region was 21.5%.

In bifacial solar cells, passivation layers are essential for reducing the recombination of minority charge carriers at the surface and achieving high efficiency and bifaciality coefficients. Different materials can be deposited to form a passivation layer and/or antireflective coating. In current technology, silicon nitride, silicon oxide, aluminum oxide and titanium oxide are the typical materials employed (Muduli and Kale, 2023). However, the most effective method for passivating crystalline silicon wafers is the use of a thermally grown silicon oxide layer. Silicon oxide thin films are usually more effective at passivating phosphorus-doped surfaces than boron-doped surfaces (Glunz and Feldmann, 2018; Bhajipale et al., 2022). On the other hand, experimental results demonstrated that a 10 nm layer of thermally grown silicon oxide passivated both doped regions, the n^+ emitter and the boron-BSF of p-type silicon solar cells (Zanesco and Moehlecke, 2015; Zanesco et al., 2017). Double layers of SiO_2/SiN_x have also been investigated (Bhajipale et al., 2022). Ultrathin silicon oxide layers have been developed for passivated contacts in TOPCon solar cells (Huang et al., 2020; Ullah et al., 2023).

Considering that bifacial solar cells represent approximately 90% of the market share and the advantages of a reduced number of thermal steps in solar cell processing, the aim of this study is to compare and analyse the bifaciality coefficients of p-type and n-type bifacial solar cells developed with the diffusion of boron and phosphorus in a single thermal step. The co-diffusion of dopants was performed according to the patent application BR1020180085760 (Zanesco and Moehlecke, 2018). This analysis enables a comparison of the potential to improve the bifaciality coefficients of n-type TOPCon and p-type PERC solar cells.

2. Bifaciality coefficients

The bifaciality coefficient affects the electrical energy produced by a bifacial photovoltaic module. This parameter is described in the IEC 60904-24 standard. Three bifaciality coefficients are defined: bifaciality coefficient of power output at the maximum power point (δ_{Pmp}), short-circuit current (δ_{Isc}), and open-circuit voltage (δ_{Voc}). The short-circuit current and maximum power output bifaciality coefficients are typically reported in the literature. The bifaciality coefficient is the ratio of the electrical parameter measured under incident irradiance on the face with lower efficiency to the electrical parameter measured under irradiance on the side with higher efficiency. In Equations (1), (2) and (3), the bifaciality coefficients are represented.

$$\delta_{Pmp} = \left[\frac{\eta_{lower-\eta}}{\eta_{higher-\eta}}\right] \quad \text{(eq. 1)}$$

$$\delta_{Isc} = \left[\frac{I_{sc_{lower-\eta}}}{I_{sc_{higher-\eta}}}\right] \quad \text{(eq. 2)}$$

$$\delta_{V_{oc}} = \left[\frac{V_{oc_{lower-\eta}}}{V_{oc_{higher-\eta}}}\right] \quad \text{(eq. 3)}$$

Considering that the sum of I_{sc} under standard test conditions with solar irradiance incident on each side independently and keeping the other side in the dark may differ from I_{sc} under simultaneous front and rear illumination, in IEC 60904-24, two methods were defined to evaluate bifacial solar cells and photovoltaic modules. In one method, the I-V curve is measured under the irradiance of 1000 W/m² on the front face (higher efficiency) and the irradiance of 135 W/m² on the rear side (lower efficiency). In the second approach, the irradiance on the rear side is increased to 300 W/m². In commercial photovoltaic modules, the maximum power output bifaciality coefficient is close to 0.70 and 0.80 for PERC and TOPCon photovoltaic modules, respectively (VDMA, 2025).

3. Materials and methods

3.1. P-type and n-type bifacial solar cell processing

Bifacial solar cells were produced in p-type and n-type Si-Cz wafers with thickness of 200 μm and resistivity ranging from 1 Ω.cm to 20 Ω.cm. The average minority carrier lifetime of p-type Si-Cz wafers was (33 ± 9) μs. This value was lower than the average minority carrier lifetime of n-type substrates, which was (79 ± 40) μs. Figure 1 shows the configuration of the bifacial n^+pp^+ and p^+nn^+ solar cells developed with a reduced number of thermal steps and silicon oxide passivation layers.

Figure 2 compares the process sequences for manufacturing bifacial solar cells by using the co-diffusion of boron and phosphorus with the baseline process using BBr_3 and $POCl_3$ as dopant sources. The boron diffusion into one side of the silicon wafers and phosphorus diffusion into the other side were carried out in a single thermal step according to the patent application BR1020180085760 (Zanesco and Moehlecke, 2018), avoiding three thermal steps and two chemical etching and cleaning steps.

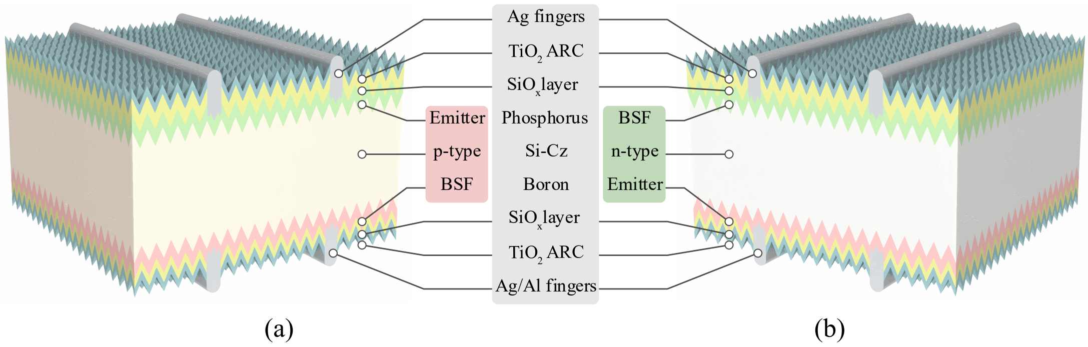

Figure 1: Configuration of the developed (a) p-type and (b) n-type bifacial solar cells with a silicon oxide layer for passivation.

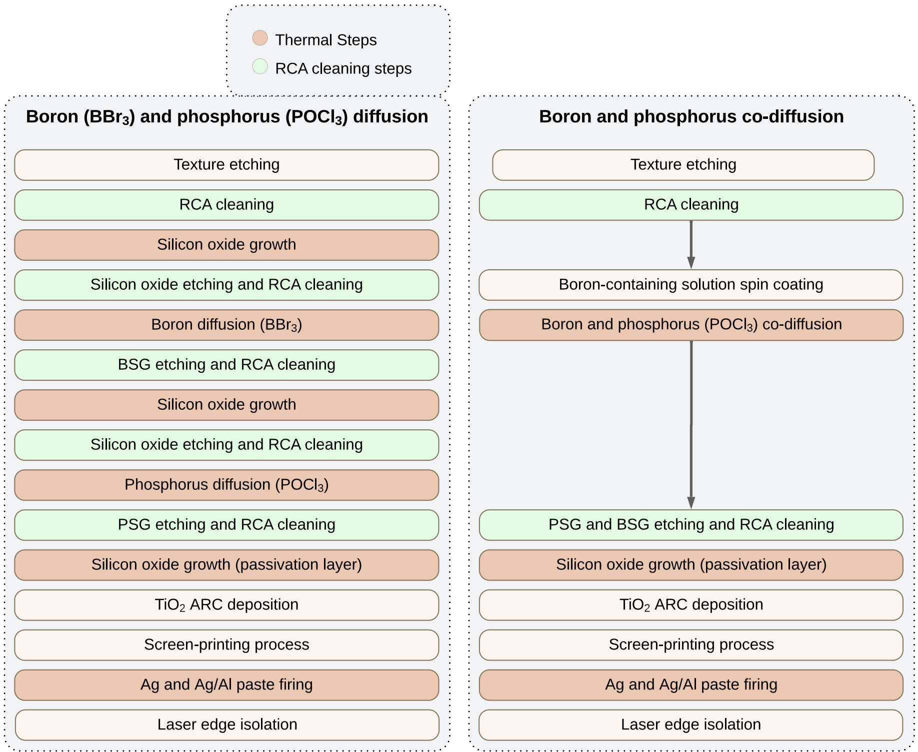

Figure 2: Comparison of the baseline process sequence with the diffusion of boron and phosphorus in a single thermal step to develop bifacial solar cells.

The solar cell processing sequence involved several steps, including texture etching in a KOH solution, RCA cleaning, deposition of a boron-containing solution (PBF20, Filmtronics) via spin-coating, diffusion of boron and phosphorus in the same thermal step in a quartz tube furnace with $POCl_3$ as the phosphorus source, borosilicate and phosphosilicate glass etching and RCA cleaning, growth of a silicon oxide layer for passivation and deposition of a TiO_2 antireflective coating on both sides of silicon wafers, screen printing of Ag and Ag/Al pastes and firing, and laser edge isolation.

Eight batches were produced. Silicon wafers were loaded into the quartz tube, and the temperature was raised to 940, 950, 960, or 970 °C for boron diffusion. In the same thermal step, the temperature was lowered to 845 °C to perform phosphorus diffusion using $POCl_3$ as the source (Wehr et al., 2019). Borosilicate glass and silicon oxide grown during boron diffusion formed a phosphorus diffusion barrier on the boron-doped side. After boron and phosphorus diffusion, borosilicate and phosphosilicate glass layers were removed in hydrofluoric acid. In the sequence, a thermal process at 800 °C was carried out to grow a silicon oxide layer on both sides for passivation (Glunz et al., 2018; Zanesco et al., 2017).

3.2. Characterization methods

The sheet resistance in a sample of each batch was measured in thirteen regions to analyse the boron-doped and phosphorus-doped layers as a function of the boron diffusion temperature. All bifacial solar cells were characterized by measuring the electric current as a function of voltage under standard test conditions (I-V curve) in a solar simulator class AAA. The I-V curve was measured under incident irradiance on one side with the other face kept in the dark to calculate and compare the bifaciality coefficients of p-type and n-type bifacial solar cells.

From the I-V curve, the short-circuit electric current density (J_{sc}), open-circuit voltage (V_{oc}), and efficiency (η) were obtained to determine the bifaciality coefficients, which were defined in the IEC 60904-24 standard. The bifaciality coefficients are analysed as a function of the sheet resistance of the boron-doped region. The maximum power output bifaciality coefficient (δ_{Pmp}) was obtained from Equation (1), and with Equations (2) and (3), the short-circuit electrical current and open-circuit voltage bifaciality coefficients were calculated.

4. Results and Discussion

4.1. Analysis of the sheet resistance of the boron-doped and phosphorus-doped layers

Figure 3 shows the average sheet resistance (R_{sh}) of the boron-doped and phosphorus-doped layers as a function of the boron diffusion temperature (T_B). As expected, the sheet resistance of the boron-doped emitter in n-type wafers and the boron-BSF in p-type substrates decreased with increasing boron diffusion temperature. This result indicated that the barrier layer for phosphorus diffusion formed in the boron-doped region was effective. However, the sheet resistance of the phosphorus-doped emitter and BSF increased as T_B increased, despite the phosphorus diffusion being performed at 845 °C in all processes. This effect is a consequence of a silicon oxide layer growing during boron diffusion on the side of the Si wafer where phosphorus diffuses in the next step, which becomes thicker with increasing T_B and acts as a barrier for phosphorus diffusion. Consequently, the sheet resistance of the phosphorus-doped emitter and BSF increased with increasing boron diffusion temperature.

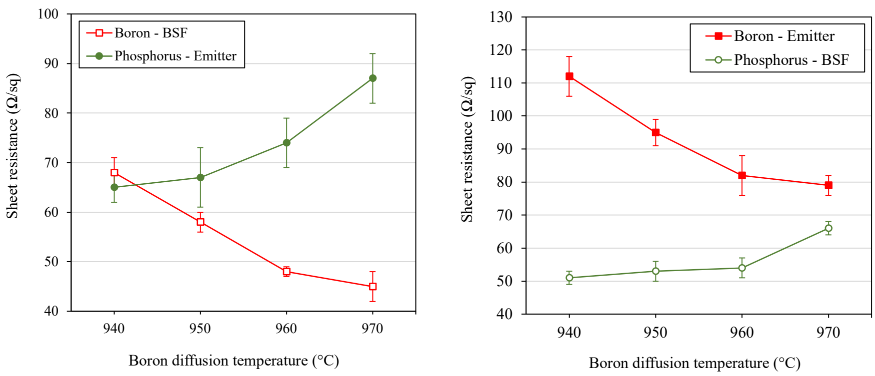

(a) (b)

Figure 3: Sheet resistance of the (a) boron-BSF and phosphorus-doped emitter produced in the p-type Si-Cz substrate and (b) boron-doped emitter and phosphorus-BSF formed in n-type Si-Cz wafers with a reduced number of thermal steps as a function of the boron diffusion temperature.

A comparison of the results presented in Figure 4 demonstrated that for both the substrates and the dopants, the sheet resistance of the emitter was higher than that of the BSF. This is a condition for producing bifacial solar cells with good performance. As Table 1 shows, in the range of boron diffusion temperatures from 940 to 970 °C, the sheet resistance of the boron-doped emitter decreased from (112 ± 6) to (79 ± 3) Ω/sq, whereas the sheet resistance of the boron-BSF ranged from (68 ± 3) to (45 ± 3) Ω/sq. The sheet resistance of the phosphorus-doped emitter layer increased from (65 ± 3) to (87 ± 5) Ω/sq. These values were higher than those measured in the phosphorus-BSF, which ranged from (51 ± 2) to (66 ± 2) Ω/sq. The results confirmed that the R_{sh} of the phosphorus-doped layer was affected by the boron diffusion temperature. The sheet resistance of n^+ regions increased by approximately 29% and 34% in the n-type and p-type samples, respectively, as the T_B increased from 940 to 970 °C.

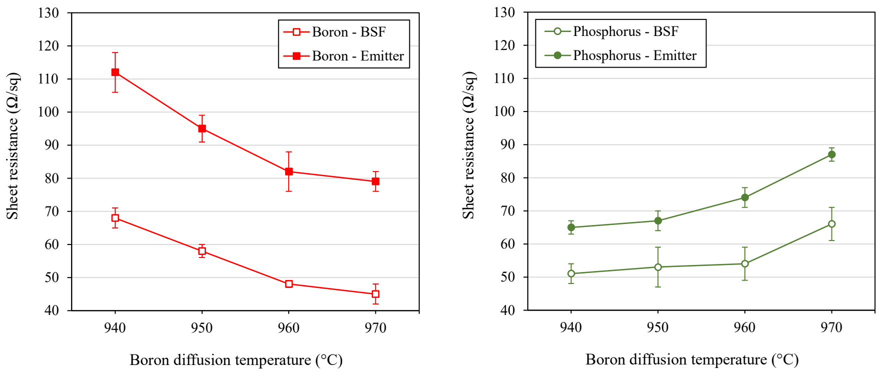

(a) (b)

Figure 4: Comparison of the sheet resistance of the (a) boron-doped emitter (n-type Si-Cz) with boron BSF (p-type Si-Cz) and (b) phosphorus-doped emitter (p-type Si-Cz) with phosphorus-BSF (n-type Si-Cz) as a function of the boron diffusion temperature.

Table 1: Average sheet resistance of the boron-doped and phosphorus-doped layers as a function of the boron diffusion temperature (T_B) produced in p-type and n-type Si-Cz substrates. Boron and phosphorus diffusions performed in a single thermal step.

	P-type Si-Cz		N-type Si-Cz	
T_B (°C)	$R_{sq\text{-}BSF}$ (Ω/sq) (boron)	$R_{sq\text{-}Emitter}$ (Ω/sq) (phosphorus)	$R_{sq\text{-}Emitter}$ (Ω/sq) (boron)	$R_{sq\text{-}BSF}$ (Ω/sq) (phosphorus)
940	68 ± 3	65 ± 3	112 ± 6	51 ± 2
950	58 ± 2	67 ± 6	95 ± 4	53 ± 3
960	48 ± 1	74 ± 5	82 ± 6	54 ± 3
970	45 ± 3	87 ± 5	79 ± 3	66 ± 2

4.2. Comparison of the bifaciality coefficients of p-type bifacial solar cells

Figure 5 shows the J-V curves of the developed p-type bifacial solar cells under incident irradiance on the phosphorus-doped emitter and boron-BSF. The short-circuit current density under boron-BSF illumination was lower than the value obtained under incident irradiance on the emitter because the higher minority carrier recombination in the p^+ BSF than in the n^+ emitter. Additionally, in bifacial solar cells, the minority carrier diffusion length should exceed twice the thickness of the solar cell (Moehlecke et al., 1995; Jimeno et al., 2007). The sample processed with a T_B of 960 °C probably has a low minority carrier lifetime and, consequently, a low minority carrier diffusion length.

Figure 5 shows that the boron diffusion temperature slightly affects the open-circuit voltage and fill factor. Consequently, the conversion efficiency and power output at the maximum power point under incident irradiance on the boron-BSF were affected mainly by the short-circuit current density. The efficiencies obtained under incident irradiance on the emitter and BSF were 16.3% and 10.2%, respectively, in p-type bifacial solar cells processed with a boron diffusion temperature of 950 °C.

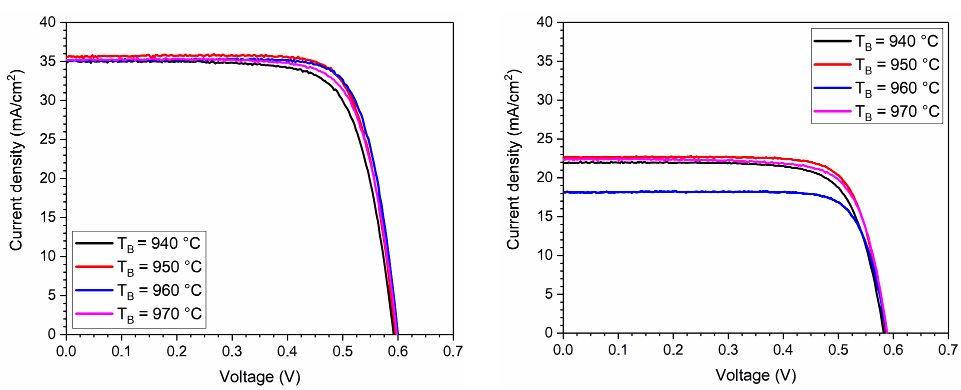

(a) (b)

Figure 5: J-V curves of the developed p-type bifacial solar cells under incident irradiance on the (a) phosphorus-doped emitter and (b) boron-BSF produced with boron and phosphorus diffusion in a single thermal step and at different boron diffusion temperatures.

The bifaciality coefficients are presented in Figure 6. Owing to the low short-circuit current density under BSF illumination, the J_{sc} bifaciality coefficient of the p-type solar cells was approximately 0.6 and slightly improved with increasing boron diffusion temperature. This result is similar to the maximum power output bifaciality coefficient reported for p-type solar cells (VDMA, 2025; Crestani et al., 2025). The open-circuit voltage bifaciality coefficient was close to 1.0 and independent of the boron diffusion temperature. Consequently, the maximum power output bifaciality coefficient was affected by δ_{Isc}.

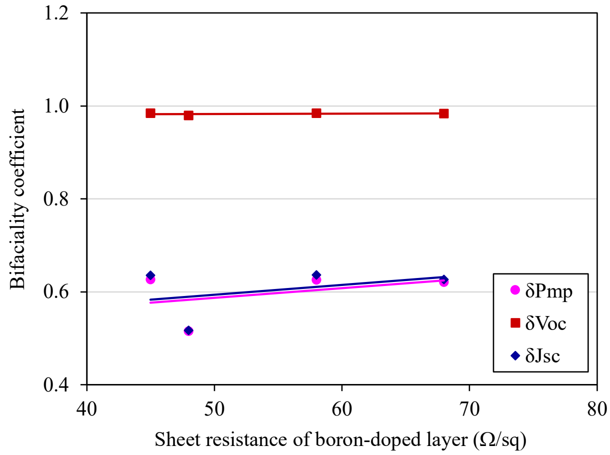

Figure 6: Bifaciality coefficients of short-circuit current density (δ_{Jsc}), open-circuit voltage (δ_{Voc}) and maximum power output (δ_{Pmp}) obtained in p-type bifacial solar cells produced with a reduced number of thermal steps as a function of the sheet resistance of the boron-BSF.

4.3. Comparison of the bifaciality coefficients of n-type bifacial solar cells

The J-V curves of bifacial n-type solar cells under incident irradiance on the boron-doped emitter and phosphorus-BSF are shown in Figure 7 (a) and (b), respectively. The J-V curves are similar, indicating that the electrical parameters are slightly affected by the incident irradiance on the emitter or BSF. The efficiency obtained under incident irradiance on the boron-doped emitter was 15.3%, which was slightly lower than the efficiency of 15.5% obtained under phosphorus-BSF illumination. This result can be explained by the lower minority carrier recombination in the phosphorus-doped region and surface. Moreover, the silicon oxide passivation layer is more effective on phosphorus-doped surfaces than on boron-doped regions, leading to lower minority carrier recombination. The solar cell with higher efficiencies was processed with a boron diffusion temperature of 960 ºC.

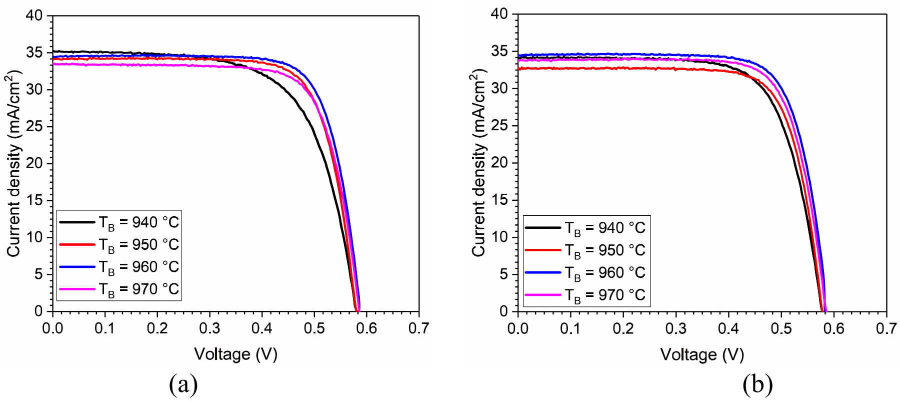

Figure 7: J-V curves of the developed bifacial n-type solar cells under incident irradiance on the (a) boron-doped emitter and (b) phosphorus-BSF produced with boron and phosphorus diffusion in a single thermal step and at different boron diffusion temperatures.

Figure 8 presents the bifaciality coefficients of the n-type bifacial solar cells. The three bifaciality coefficients were close to 1.0. For this type of silicon substrate, the maximum power output bifaciality coefficient tended to decrease with increasing boron diffusion temperature. Nevertheless, the short-circuit current bifaciality coefficient slightly increased. As the open-circuit voltage bifaciality coefficient remained close to 1.0, δ_{Pmp} was affected by the fill factor, which decreased with increasing sheet resistance of the boron-doped emitter because of the augment in contact resistance.

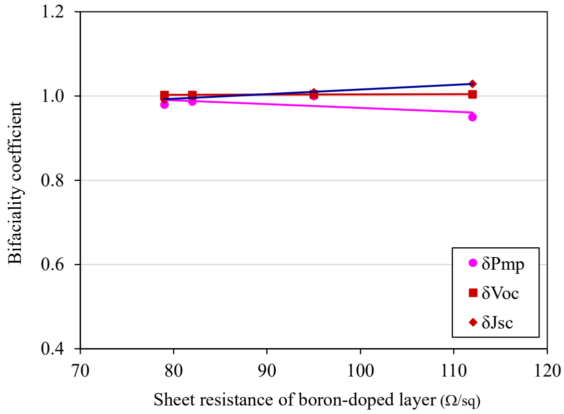

Figure 8: Bifaciality coefficients of short-circuit current density (δ_{Jsc}), open-circuit voltage (δ_{Voc}) and maximum power output (δ_{Pmp}) obtained in n-type bifacial solar cells produced with a reduced number of thermal steps as a function of the sheet resistance of the boron-doped emitter.

4.4. Comparison of the bifaciality coefficients of p-type and n-type bifacial solar cells

A comparison of Figure 7 (a) with Figure 7 (b) reveals that the short-circuit current density measured under emitter or BSF illumination was similar in solar cells produced in the n-type substrate. However, in p-type bifacial devices, the short-circuit current density under incident irradiance on the boron-BSF was 37% lower than the J_{sc} under emitter illumination. The efficiency under incident irradiance on the emitter was higher in p-type solar cells than in n-type bifacial devices. On the other hand, the efficiency of n-type solar cells under phosphorus-BSF illumination was higher than the value obtained under emitter illumination and was 52% (relative) greater than the efficiency measured in p-type solar cells under incident irradiance on the boron-BSF.

Figure 9 compares the bifaciality coefficients as a function of the sheet resistance of the boron-doped layer. The bifaciality coefficients of the n-type solar cells were close to 1.0. Nevertheless, the J_{sc} bifaciality coefficient of the p-type devices was low, indicating higher minority carrier recombination in the pp^+ region than in the nn^+ layer.

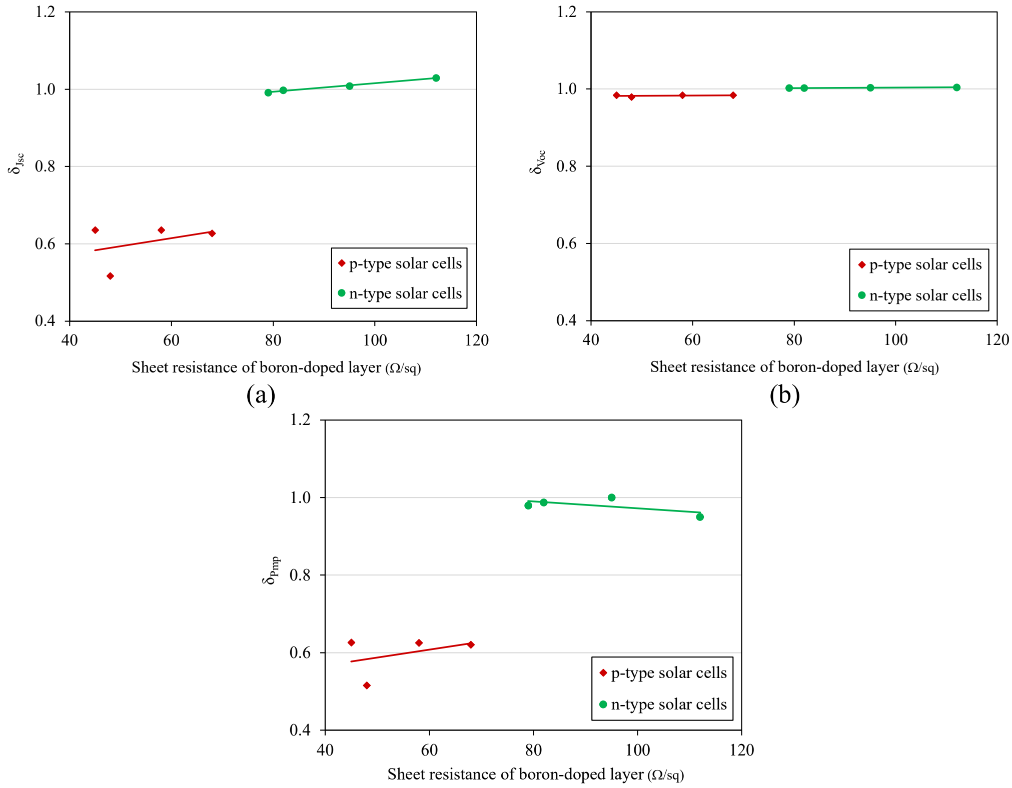

(c)

Figure 9: Comparison of the bifaciality coefficients of (a) short-circuit current density (δ_{Jsc}), (b) open-circuit voltage (δ_{Voc}) and (c) maximum power output (δ_{Pmp}) obtained in p-type and n-type bifacial solar cells as a function of the sheet resistance of the boron-doped layer.

The δ_{Pmp} obtained in p-type solar cells was 0.62–0.63, similar to the value of 0.7 reported for solar cells passivated with a silicon oxide layer (Crestani et al., 2025). For both substrate types, δ_{Isc} tended to increase with increasing sheet resistance of the boron-doped layer because of the lower minority carrier recombination in the doped region. The open-circuit voltage bifaciality coefficient was close to 1.0, and this parameter was slightly lower for p-type solar cells. For this substrate, δ_{Isc} affected the maximum power output bifaciality coefficient. A different behaviour was observed for the maximum power output bifaciality coefficient of the n-type solar cells, which tended to decrease with increasing sheet resistance of the boron-doped layer.

In summary, the limiting factor of the short-circuit current density and maximum power output bifaciality coefficients of p-type bifacial PERC solar cells is the high carrier recombination in the boron-doped pp^+ region and surface. However, the high bifaciality coefficients obtained in n-type solar cells demonstrated that commercial n-type TOPCon solar cells have the potential to achieve high bifaciality coefficients and that the δ_{Pmp} can be improved from 0.8 to approximately 1.0.

Another way to increase the bifaciality coefficient of silicon solar cells is to reduce the thickness of the silicon wafer to increase the ratio of the minority carrier diffusion length to the thickness. The resistivity of the silicon wafer also affects the bifaciality coefficients. Substrates with higher resistivity result in greater bifaciality coefficients. To obtain a δ_{Isc} of 0.9 with the n^+pp^+ structure, the resistivity of the crystalline silicon substrate must be greater than 20 Ω.cm, and the minority carrier lifetime must be higher than 200 µs (Moehlecke et al., 1995).

5. Conclusions

The analysis of the sheet resistance of the boron-doped layer revealed higher values for the emitter in the n-type substrate than for BSF in the p-type substrate. In the range of boron diffusion temperatures from 940 to 970 °C, the sheet resistance of the boron-doped emitter in the n-type Si wafers decreased from (112 ± 6) to (79 ± 3) Ω/sq, whereas in the p-type substrate, the sheet resistance of the BSF ranged from (68 ± 3) to (45 ± 3) Ω/sq. The sheet resistance of the phosphorus-doped emitter was also higher than the value of phosphorus BSF, and R_{sh} was affected by the boron diffusion temperature. The sheet resistance of the phosphorus-doped layer increased by approximately 29% and 34% in the n-type and p-type samples, respectively, with increasing boron diffusion temperature.

In p-type bifacial solar cells, the short-circuit current density under incident irradiance on the boron-BSF was 37% lower than the J_{sc} under emitter illumination. Nevertheless, for n-type solar cells, the short-circuit current density was similar for both illumination modes. The boron diffusion temperature slightly affected the open-circuit voltage and fill factor. Consequently, the conversion efficiency and power output at the maximum power point with irradiance on the boron-BSF were affected mainly by the short-circuit current density in p-type bifacial solar cells. The efficiencies obtained under incident irradiance on the emitter were 16.3% and 15.3% for p-type and n-type bifacial solar cells, respectively. Therefore, the diffusion of boron and phosphorus in a single thermal step successfully produced n-type and p-type bifacial solar cells with a reduced number of thermal steps.

Owing to the low short-circuit current density under BSF illumination, the J_{sc} bifaciality coefficient of the p-type devices was approximately 0.6 and slightly improved with increasing boron diffusion temperature. The open-circuit voltage bifaciality coefficient was close to 1.0, and consequently, the maximum power output bifaciality coefficient was affected by δ_{Isc}. Otherwise, the bifaciality coefficients of the n-type solar cells were close to 1.0. In this type of substrate, the maximum power output bifaciality coefficient tended to decrease with increasing boron diffusion temperature, and in p-type solar cells, this parameter increased with T_B.

The J_{sc} bifaciality coefficient of the p-type bifacial solar cells was lower than that of the n-type devices because of higher carrier recombination in the pp^+ BSF than in the nn^+ BSF. Therefore, carrier recombination in the boron BSF region and surface is the limiting factor of the short-circuit current density and maximum power output bifaciality coefficients of p-type bifacial PERC solar cells. On the other hand, the n-type TOPCon configuration has the potential to achieve high bifaciality coefficients, and these parameters may be improved from 0.8 to approximately 1.0 in commercial devices.

6. Acknowledgements

The authors acknowledge the financial support of the Funding Authority for Studies and Projects (FINEP), grant number 01.22.0194.00, and the National Council for Scientific and Technological Development (CNPq), grant numbers 305554/2021-2, 440046/2019-0 and 306916/2017-7.

7. References

Arndt, R.A., Allison, J.F., Haynos, J.G., Meulenberg, A., 1975. Optical properties of the COMSAT non-reflective cell. In: 11th IEEE Photovoltaic Specialists Conference, p. 40.

Bhajipale, J., Mitra, S., Ghosh, H., Sreejith, K.P., Kottantharayil, A., 2022. Spray-coated SiO_2/PECVD SiN_x stack for the passivation of n^+ emitter of p-type Si solar cell. Solar Energy 246, 113–118. https://doi.org/10.1016/j.solener.2022.08.025

Crestani, T., Zanesco, I., Moehlecke, A., Pires da Silva, L.T.C., Britto, J.V.Z., 2025. Optimization of the boron back surface field produced with reduced thermal steps in bifacial PERT solar cell. Energies 18, 2347. https://doi.org/10.3390/en18092347

Cuevas, A., 2005. The early history of bifacial solar cells. In: 20th European Photovoltaic Solar Energy Conference and Exhibition (EU PVSEC), Barcelona, Spain, pp. 172–175.

Feng, J., Yu, B., He, Y., Lv, A., Fan, J., Yang, L., Xia, Z., Li, Z., Meng, X., Jiang, F., Xing, G., Yu, J., 2025. Enabling 95% bifaciality of efficient TOPCon solar cells by rear-side selective sunken pyramid structure and zebra-crossing passivation contact. Solar Energy Materials & Solar Cells 292, 113809. https://doi.org/10.1016/j.solmat.2025.113809

Green, M.A., 2015. The passivated emitter and rear cell (PERC): From conception to mass production. Solar Energy Materials and Solar Cells 143, 190–197. https://doi.org/10.1016/j.solmat.2015.06.055

Glunz, S.W., Knobloch, J., Biro, D., Wetting, W., 1997. Optimized high-efficiency silicon solar cells. In: 14th European Photovoltaic Solar Energy Conference and Exhibition (EU PVSEC), June, Barcelona, pp. 392–395.

Glunz, S.W., Feldmann, F., 2018. SiO_2 surface passivation layers – a key technology for silicon solar cells. Solar Energy Materials and Solar Cells 185, 260–269. https://doi.org/10.1016/j.solmat.2018.04.029

Huang, Y., Liao, M., Wang, Z., Guo, X., Jiang, C., Yang, Q., Yuan, Z., Huang, D., Yang, J., Zhang, X., Wang, Q., Jin, H., Al-Jassim, M., Shou, C., Zeng, Y., Yan, B., Ye, J., 2020. Ultrathin silicon oxide prepared by in-line plasma-assisted N_2O oxidation (PANO) and the application for n-type polysilicon passivated contact. Solar Energy Materials and Solar Cells 208, 110389. https://doi.org/10.1016/j.solmat.2019.110389

Huang, Y., Jiang, L., Yan, L., Yang, Y., Chen, R., Cui, H., et al., 2024. A novel phosphorus diffusion process for front-side p–n junction fabrication in PERC solar cells. Materials Science in Semiconductor Processing 180, 108552. https://doi.org/10.1016/j.mssp.2024.108552

Ingenito, A., Allebé, C., Libraro, S., Ballif, C., Paviet-Salomon, B., Nicolay, S., Diaz Leon, J.J., 2023. 22.8% full-area bifacial n-PERT solar cells with rear side sputtered poly-Si(n) passivating contact. Solar Energy Materials and Solar Cells 249, 112043. https://doi.org/10.1016/j.solmat.2022.112043

Jimeno, J.C., Bueno, G., Lago, R., Freire, I., Pérez, L., Recart, F., Hoces, I., Azkona, N., Alonso, J., Sánchez-Friera, P., Glunz, S.W., Emanuel, G., Ruiz, R., Pohl, A., Wolke, W., Schubert, M., Gavilanes, I., Ezker, M., Zugasti, E., Turumbay, A., Sato, H., Bragagnolo, J., Nasch, P.M., Ostapenko, S., Belyaev, A., Dallas, W., Polupan, O., Albertsen, K., Shaikh, A., Kerp, H., Salami, J., 2007. Low cost using ultra-thin bifacial cells. In: 22nd European Photovoltaic Solar Energy Conference and Exhibition (EU PVSEC), Milan, pp. 1–4.

Kafle, B., Goraya, B.S., Mack, S., Feldmann, F., Nold, S., Rentsch, J., 2021. TOPCon – Technology options for cost-efficient industrial manufacturing. Solar Energy Materials and Solar Cells 227, 111100.

Khelifati, N., Charif, I, Bouhafs, D., Palahouane, B., Mahmoudi, B., Saddik-El-Hak, A., 2020. Phosphorus and boron co-diffusion in silicon for p-PERT solar cells application. In: 2020 IEEE International Conference.

Linke, J., Peter, C., Hoß, J., Sharbaf Kalaghichi, S., Mihailetchi, V., Lossen, J., et al., 2025. 24% efficient TOPCon-based back-contacted poly-ZEBRA solar cells. EPJ Photovoltaics 16, 8. https://doi.org/10.1051/epjpv/2024051

Macdonald, D., 2012. The emergence of n-type silicon for solar cell manufacture. In: Proceedings of the 50th Annual AuSES Conference (Solar), Melbourne, Australia, pp. 1–6.

Moehlecke, A., Zanesco, I., Luque, A., 1994. Practical high-efficiency bifacial solar cells. In: First World Conference on Photovoltaic Energy Conversion (WCPEC), 5–9 December, Hawaii.

Moehlecke, A., Zanesco, I., Cañizo, C., Luque, A., 1995. Experimental comparison between p and n bases for bifacial solar cells. In: 13th European Photovoltaic Solar Energy Conference and Exhibition (EU PVSEC), Nice, France, pp. 1242–1245.

Muduli, S.P., Kale, P., 2023. State-of-the-art passivation strategies of c-Si for photovoltaic applications: A review. Materials Science in Semiconductor Processing 154, 107202. https://doi.org/10.1016/j.mssp.2022.107202

Sugiura, T., Matsumoto, S., Nakano, N., 2021. Bifacial PERC solar cell designs: bulk and rear properties and illumination condition. IEEE Journal of Photovoltaics 10(6), 1538–1544. https://doi.org/10.1109/JPHOTOV.2020.3013987

Ullah, H., Czapp, S., Szultka, S., Tariq, H., Bin Qasim, U., Imran, H., 2023. Crystalline silicon (c-Si)-based tunnel oxide passivated contact (TOPCon) solar cells: A review. Energies 16, 715. https://doi.org/10.3390/en16020715

VDMA, 2025. International Technology Roadmap for Photovoltaics (ITRPV), 16th ed. VDMA, Frankfurt am Main, Germany.

Wang, Q., Guo, K., Gu, S., Huang, W., Peng, H., Wu, W., et al., 2024. Electrical performance, loss analysis, and efficiency potential of industrial-type PERC, TOPCon, and SHJ solar cells: A comparative study. Progress in Photovoltaics: Research and Applications 32, 889–903. https://doi.org/10.1002/pip.3839

Wang, Q., Guo, K., Wu, W., Gu, S., Zhang, X., Cao, J., et al., 2025. 26.35%-efficiency and high-bifaciality n-TOPCon solar cells enabled by UV-ps laser-induced selective modification of double-layered SiO_x/n^+-poly-Si passivating contacts. Energy & Environmental Science, advance online publication (26 Sep 2025). https://doi.org/10.1039/D5EE02742J

Wehr, G., Zanesco, I., Moehlecke, A., 2019. Influence of diffusion parameters on electrical characteristics of mc-Si solar cells with aluminum and phosphorus diffusion performed in the same thermal step. Materials Research 22. https://doi.org/10.1590/1980-5373-mr-2018-0443

Wei, Q., Zhang, S., Yu, S., Lu, J., Lian, W., Ni, Z., 2017. High-efficiency n-PERT solar cells by B/P co-diffusion method. Energy Procedia 124, 700–705.

Wei, P., Tong, R., Liu, X., Wei, Y., Zhang, Y., Liu, X., Dai, J., Yin, H., Liu, D., 2024. Optimization of rear-side passivation for enhancing the performance of bifacial $PERC^+$ solar cells. Materials Science in Semiconductor Processing 170, 107947. https://doi.org/10.1016/j.mssp.2023.107947

Yin, H.P., Tang, K., Zhang, J.B., Shan, W., Huang, X.M., Shen, X.D., 2020. Bifacial n-type silicon solar cells with selective front surface field and rear emitter. Solar Energy Materials and Solar Cells 208, 110345.

Yuan, D., Cui, J., Ding, J., Zhong, C., 2025. Efficiency loss analysis and simulation of 23.2% efficiency PERC cell. Optical and Quantum Electronics 57, 216. https://doi.org/10.1007/s11082-025-08136-w

Zanesco, I., Moehlecke, A., 2015. Analysis of the silicon dioxide passivation and forming gas annealing in silicon solar cells. In: ISES Solar World Congress 2015, Daegu, pp. 1–9.

Zanesco, I., Razera, R.A.Z., Moehlecke, A., 2017. Analysis of SiO_2 passivation layer in the rear and front face of solar cells with selective back surface field. Revista Matéria 22, 1–9. https://doi.org/10.1590/S1517-707620170005.0260

Zanesco, I., Moehlecke, A., 2018. Diffusion process of p-type and n-type dopants in silicon wafers in the same thermal step. Brazilian patent BR1020180085760. Patent application: 2018; PCT: 2019. Patent applicants: Eletrosul Centrais Elétricas S.A. and PUCRS.

Zhang, C., Shen, H., Sun, L., Yang, J., Wu, S., 2020. Bifacial p-type PERC solar cell with efficiency over 22% using laser-doped selective emitter. Energies 13, 1388. https://doi.org/10.3390/en13061388

Zhou, Z., Kang, Q., Sun, Z., He, Y., Li, J., Sun, C., Xue, C., Qu, M., Chen, X., Zheng, Z., Wang, B., Yan, H., Xu, X., Zhang, Y., 2024. Optimizing strategy of bifacial TOPCon solar cells with front-side local passivation contact realized by numerical simulation. Solar Energy Materials & Solar Cells 278, 113189. https://doi.org/10.1016/j.solmat.2024.113189